Author(s): Sippola, Merja; Immonen, Kirsi; Miettinen, Arttu; Laukkanen, Anssi; Andesson, Tom; Peltola, Heidi; Harlin, Ali; Holmberg, Kenneth

Title: Predicting stiffness and strength of birch pulp : polylactic acid composites

Year: 2016

Version:

Predicting stiffness and strength of birch pulp – polylactic acid composites

Merja Sippola[1], Kirsi Immonen[2], Arttu Miettinen[3], Anssi Laukkanen[1], Tom Andersson[1], Heidi Peltola[2], Ali Harlin[4] and Kenneth Holmberg[5]

[1] Material modeling and ecodesign, VTT Technical Research Centre of Finland, Finland

[2] Biocomposites and processing, VTT Technical Research Centre of Finland, Finland

[3] Department of Physics, University of Jyväskylä, Finland

[4] Process chemistry and environmental engineering, VTT Technical Research Centre of Finland, Finland

[5] Materials performance, VTT Technical Research Centre of Finland, Finland

Corresponding author:

Merja Sippola, Material modeling and ecodesign, VTT Technical Research Centre of Finland, Finland

Email: merja.sippola@vtt.fi

Phone: +358503287001

Abstract

This paper studies failure of birch pulp – polylactic acid (PLA) composites. Stiffness and strength are calculated using the theory of short fibre composites and the results are compared to experimental data. The results differed from the experimental values by 0 - 6 %. With less aligned fibres the short fibre theory is not feasible. The performance of the 40 wt% birch pulp – PLA composite is predicted with X-ray micro tomography (X-μCT) based Finite Element Modelling (FEM), and the results are compared with experiments. Stiffness results differed from experiments by 1 - 17 % . By adding into the models a third material phase representing the interface between the fibres and the matrix, the stress-strain curve of the composite was obtained with good accuracy. The work presents FEM methodology of Wood Plastic Composites (WPCs) and the critical further steps needed in order to assess the stress-strain behaviour, strength and stiffness. Tools for comparing different WPC microstructures are also presented.

Keywords

Introduction

Polymer composites containing wood based cellulose fibres, WPCs (Wood Plastic Composites) are promising materials for various applications utilised in injection moulding, extrusion or compression moulding. The advantages of wood fibres over other plant based cellulose fibres are their low cost, uniform quality, good availability

and the ability to use preforms manufactured with paper making technology. Additionally wood fibres do not compete with food cultivation. WPCs have low density, low equipment abrasion caused by wood fibres and WPCs can be easily surface modified.[1, 2]

An often applied biodegradable polymer is stereoselective polylactic acid (PLA), one of the stereoisomers of polylactic acid.[1] PLA is an interesting bio-based polymeric matrix due to its biodegradability, sealing ability, high tensile strength properties and good availability. The mechanical properties are similar or better than those of e.g. polypropylene, which makes it attractive in single use packaging applications. It has, however, also some limiting properties such as low thermal stability and brittleness. Those have been improved by e.g. addition of natural fibres to the polymer.

Wood fibres are naturally hydrophilic. This and the resulting poor bond with hydrophobic matrix make the material susceptible to moisture and reduce the strength of the composite. It is also difficult to gain good dispersion of the fibres to the polymers. Short fibre length (0.2 – 0.8 mm) also limits achievable material strength. Literature presents several methods to improve dispersion and fibre polymer interaction through fibre selection, chemical and physical modifications and coupling agents [3, 4]. Wood fibre-PLA interphase is studied in several papers by Almgren, who has utilised Halpin-Tsai's and Hashin and Rosen's viscoelastic models and studied moisture behaviour of fibres and fibre-fibre interaction effect on composite properties.[5] Peltola et al. studied plastic processing and dispersion of various wood cellulose fibre types in PLA and PP composites and found out that fibres disperse better in PLA, but are going through quite high fibre length reduction due to processing.[6] Chinga-Carrasco et al.[7] applied X-ray micro tomography (X-μCT) to injection moulded PLA-kraft pulp

composites and found it to be the most appropriate method for exploring the surface and bulk structures of fibre-reinforced composites non-destructively. The results revealed a significant reduction of the fibre length from >1500 μm to <200 μm in the process, which could impose a limitation in the proper application of wood fibres as reinforcement in biodegradable composites.

Predictions regarding the performance of short fibre composites with various methods have been applied before by other research groups. Joffre [8] studied structure and the hygroelastic behaviour of wood fibre composites utilising X-μCT and FEM (Finite Element Method). Micromechanics of the bond between wood fibres and polymer matrices with X-μCT and the Material Point Modelling (MPM) method has been investigated by Schwarzkopf et al. [9, 10] Imperfect bond is one of the two most critical issues affecting strength of WPCs. The other is the length of the fibres. Madsen et al. [11] assessed stiffness and strength of cellulosic fibre - starch acetate composites with the short fibre theory. Eitzenberger [12] and Lu [13] have written good reviews on the methods for predicting stiffness and strength of short fibre composites. There are many different methods for predicting stiffness [14, 15, 16, 17, 18, 19, 20, 21, 22, 23], but most of the methods work well only for small fibre volume fractions. Pan's method [20] has no restriction for fibre volume fraction and was chosen for stiffness prediction in the present work.

Several researchers have studied failure of short fibre composites. Curtis et al. [21] used modified rule of mixtures and Cox's shear lag analysis [22]. Kelly and Tyson [23] used an extension of the rule of mixtures by taking into account both fibre length and fibre orientation. Fu and Lauke [24] studied effects of fibre length distribution and fibre angle distribution on the strength of short fibre composites. They studied fibre breaking and

fibre pull-out. Chen [22] started from the potential failure modes of continuous fibre composites and took the fibre length into account by length efficiency factor and fibre orientation into account by considering coordinate transformation of stresses in an orthotropic material.

This paper studies the failure of birch pulp – PLA composites without chemical or physical modification aiming at modelling the tensile strength properties of the composites. The starting points are fibre length and radius distributions obtained by a fibre analyser, Scanning Electron Microscopy (SEM) images of the composites and on the other hand X-ray microtomographic (X-µCT) pictures of injection moulded composites. The stiffness and strength of the composites are studied by tensile tests, analytical methods and X-ray tomography based Finite Element Modelling. The aim of the paper is to present the modern methodology of modelling stiffness and strength of WPCs as well as to critically assess the potential and the limitations of these methods in relation to WPCs and to point out the most important further work needed in computer-assisted design and tailoring of strong and durable WPCs.

Materials and methods

Material processing

The PLA - birch cellulose composites were prepared using PLA from Hycail (HM 1011, melt flow rate 2-4 g/10 min) and bleached cellulose pulp from Metsä Botnia without modifications. Pulp was dried 12 h in 50°C before compounding to the moisture content below 2%. The materials were compounded before injection moulding to ensure the proper mixing of materials using co-rotating Berstorff ZE 25x33D compounder to

5

20 wt% and 40 wt% fibre contents. Compounding of pulp and polymer was made with temperature gradient 160-195 °C and injection moulding with temperature gradient 170-195°C. In injection moulding the mould temperature was 27 °C and pressure 80-120 bar. They were injection moulded to standard shaped tensile test pieces (i.e. 'dog bone specimens', see Figure 1) with Engel ES 200/50 HL injection moulding machine.

SEM analysis

The morphology of injection moulded samples were studied by scanning electron microscope (SEM) from the cross-section of the sample. In order to get good visibility surfaces for SEM imaging the sample was cooled in liquid nitrogen and broken in two. The sample surface was coated with gold to prevent charging of the surface. The imaging was made using JEOL JSM T100 in secondary electron mode with an acceleration voltage of 25 kV.

Fibre analysis

To determine the fibre dimensions of the injection moulded composites, the polymer matrix was dissolved from the test samples. PLA was dissolved with methylene chloride by heating the chemical to its boiling point (39.8°C) and the dissolved components were filtered with glass sinters and washed with methylene chloride. The dimensions (length, width, aspect ratio and fines proportion) of the remaining fibres were analysed using the automated fibre analyser L&W STFI FibreMaster (FM).

X-*ray micro tomography*

Micro tomographic images were created from a small piece of the 40 wt% birch pulp – PLA composite. For X-ray micro tomographic imaging, cylindrical sample of approximately 1.1 mm diameter was cut from the composite material using a rotary

tool. The sample was glued onto the top of a sample holder rod and a tomographic image was acquired using XRadia µCT-400 device with 1.2 µm resolution, 30 kV acceleration voltage and 3 W X-ray power. A tomographic slice through the material is shown in Figure 6.

Tensile testing

Tensile testing was performed according to SFS-EN ISO 3167:2003 using Instron 4505 mechanical test equipment. The samples were dog bone-shaped standard samples and five parallel samples were tested.

Material characteristics

Tables 1 and 2 list the material parameters for the 40 % and 20 % birch pulp – PLA composites, respectively. The Young's modulus of the fibres was assumed to be 37 GPa based on the wood species and density. The original reference was a web page by Neagu 15.12.2009, where the values ranged between 32 and 42 GPa. This web page is not found on the net any more, but in a paper by Neagu et al the Young's modulus for birch pulp fibre was about 38 GPa. [25] The Young's modulus of the matrix was measured by tensile testing of pure PLA. The Poisson ratios were assumed 0.3 for the matrix and 0.2 for the fibres. The shear modulus of the matrix was calculated using the isotropy assumption. The critical interfacial shear stress between fibres and matrix τ_c was assumed based on Zhang's results. [26] The strength of the matrix was measured by tensile testing pure PLA. The strength of the fibres was taken from studies from Roberts et al. [27]. The average fibre angle for each composite was obtained from SEM images manually. The result is very approximate. More exact information could be derived

from micro tomography but that was not possible in this small project. The fibre length

distributions were combined from the FM and SEM analysis results.

Theoretical consideration

In the composites of the current study the fibres are weakly oriented. The average fibre

angle θ_{avg} (the angle between the loading direction and the fibre) is about 46 degrees

for the 40 % birch pulp – PLA composite and about 30 degrees for the 20 % birch pulp

– PLA composite. For stiffness calculation both composites can be approximated by a

two-dimensional (2D) random composite.

According to Pan [20] the stiffness of a 2D random short fibre composite in the loading

direction is

$$E_1 = E_f \frac{V_f}{\pi} + E_m (1 - \frac{V_f}{\pi}) \qquad (1)$$

where E_f is the fibre stiffness,

E_m is the matrix stiffness,

V_f is the fibre volume fraction and

V_m is the matrix volume fraction.

For a 2D random composite the stiffness in the transverse direction is the same

$$E_2 = E_1 \qquad (2)$$

The Poisson's ratio is approximated by

$$v_{12} = v_f \frac{V_f}{\pi} + v_m (1 - \frac{V_f}{\pi}) \qquad (3)$$

where v_f is the Poisson's ratio of the fibre and

8

v_m is the Poisson's ratio of the matrix

Taking into account (2)

$$v_{21} = v_{12} \tag{4}$$

In a 2D random composite the shear modulus can be calculated analogously to isotropic materials

$$G_{12} = \frac{E_1}{2(1+v_{12})} \tag{5}$$

According to Chen [22] if the (average) fibre angle is small (most of) the fibres break first; if the fibre angle is large the matrix fails first in tension; at intermediate angles the interface fails in shear.

In the composites of this study the fibres are very short and the interface is rather weak. Both these factors promote interface failure.

In most studies of strength of short fibre composites the fibres are assumed fully oriented in the direction of the loading. In the common simplification [12] of the shear lag model originally proposed by Cox [14] the stress in the matrix is transferred to the fibres according to equation (6)

$$\frac{d\sigma_f}{dx} = \tau \frac{2}{r} \tag{6}$$

where σ_f is the axial stress in the fibre,

τ is the shear stress at the fibre interface

and r is the fibre radius.

If it is assumed that the shear stress is constant τ_c, integration of equation (6) gives

$$\sigma_f = x \frac{2\tau_c}{r} \tag{7}$$

where x is the distance from the fibre end.

This means that the axial stress changes linearly at the fibre ends.

If the strength of the fibre is σ_f^* then critical fibre length needed for the fibre to break is

$$l_c = \sigma_f^* \frac{r}{\tau_c} \tag{8}$$

The length, radius and critical length distributions of the 40 % birch pulp - PLA composite are shown in Table 3 and the corresponding distributions of the 20 % birch pulp – PLA composite in Table 4.

If the fibres are long enough for the stress to be fully transmitted to the fibre so that the fibres break before the bond between the fibre and matrix fails or the matrix itself fails, the strength of the composite is according to equation (9) [12]

$$\sigma_c^* = \sigma_f^* (1 - \frac{l_c}{l}) V_f + \sigma_m' V_m \tag{9}$$

where

l is the fibre length and

σ_m' is the stress in the matrix when the fibre breaks.

If the length of the fibre is below the critical length the fibres don't break, but the bond fails and the fibres are pulled out. The strength of the composite is then

$$\sigma_c^* = V_f \frac{l\tau_c}{2r} + V_m \sigma_m^* \tag{10}$$

where σ_m^* is the matrix strength.

In the current study the governing failure mechanism in the more oriented 20 % birch pulp – PLA composite is assumed to be fibre breaking. While calculating strength the fibres are assumed to be fully oriented. The strength was first calculated for each composite fraction corresponding to an identified fibre length fraction separately (using the middle value of the fraction as the fibre length) and then a weighted average was calculated. In the less oriented 40 % birch pulp – PLA composite the governing mechanism is assumed to be interface failure. Bond failure at the fibre-matrix interface can be a shear failure along the fibre, an opening mode failure at the interface due to tensile stress transverse to the fibre or a mixed mode failure due to the combination of shear stress and transverse-to-the-fibre tensile stress. Local stress concentrations at the fibre-matrix interface due to the difference in the elastic moduli between the matrix and the fibre promote interface failure.

If the angle θ_{avg} is large, the interface failure can be considered opening mode failure due to the transverse-to-the-fibre tensile stress. If the angle is small, the failure can be considered shear failure due to the shear stress transferring the load to the fibre. In that case the shear stress caused by the fibre angle is small. At intermediate cases both (local and global) shear stress components and the tensile stress transverse to the fibre all affect the failure at the interface.

In the 40 % birch pulp – PLA composite the angle θ_{avg} is large and the interface is relatively weak. Thus the likely failure mode is interface failure in transverse tension. The yield strength of the composite is reached when the fibres start to de-bond, which shows as a sudden or gradual change in the slope of the stress-strain curve. The change is more sudden if the fibres are well aligned along the loading direction. If the fibre alignment is more random, the bond of differently aligned fibres breaks at different load

and thus the change in the slope is gradual. Breaking of fibres can also cause gradual degradation of stiffness if the fibre angles and fibre lengths vary a lot.

Modelling

Building up of numerical finite element models, mesh modification steps and statistical post-processing of results was carried out following and adapting methodologies presented in relation to the VTT ProperTune multiscale modelling toolset [28, 29], previously applied to various different kinds of composite material microstructures. In the current work 2D FE meshes were created from the micro tomographic images by the OOF2 program [30] preceded by segmentation to a binary image. The first models contained two phases, the matrix and the fibres. The meshes were further processed and smoothened after the initial discretization, which aims at meeting the criteria set for the image based discrete phase distribution, to improve mesh quality and remove element features impairing the numerical computations. In order to better model the stress-strain behaviour a third phase was added at the border of fibres and matrix with image analysis tools. This model is an effective interface model, where an interface region and phase of finite thickness is introduced to capture the mechanical response of the interface region. In essence, it can be viewed also as a mean field approximation of the actual smaller spatial scale interface features. The interface region is created by first identifying all phase boundaries from the processed image, and subsequently adding a finite thickness layer in between phases by directly modifying the pixel structure. In current work a symmetric interface with respect to the interface polyline was created on

the basis of available image resolution, adding a single pixel/voxel to each side of the interface to obtain the finite thickness layer.

Figure 6 shows one slice through the stack in the micro tomographic volume image. Slices at locations ¼, ½ and ¾ of the specimen thickness were chosen and 2D FE meshes were created. Quad meshes, triangular meshes and mixed meshes were made with linear elements. The stiffness of the matrix was 3771 MPa (average of experimental values with variation ±150 MPa). The stiffness of the fibres was varied between 30 and 42 GPa. The 3D Poisson's ratio of the matrix was assumed 0.3 and the 3D Poisson's ratio of the fibres 0.2. The different meshes gave very similar results and most of the models were made with a mixed mesh. Figure 7 shows a mixed FE mesh of the slice image (in Figure 6).

In later models a third material phase was created between the fibres and the matrix utilising modern image analysis tools (see Figure 9). A plastic model created from an experimental stress-strain curve of PLA was used for the matrix and the border phase (see Table 5). The elastic modulus of the PLA matrix was taken as 3771 MPa. As the image analysis based creation of the border phase took some area from inside the fibres as well as area inside the matrix, and also it is unknown how much of the fibre surface is bonded to the matrix, the correct stress-strain curve was fitted by varying the elastic moduli of the fibres between 30 and 50 GPa and the border phase between 1000 MPa (representing nearly no bond) and 11 GPa (representing strong bond and compensating for the lost area of the fibres).

Results

Experimental results

Prior to modelling, fibre dimensions, morphologies and the mechanical performance of the composites were analysed. The fibre length and radius distributions of the 40 % birch pulp- PLA composite are shown in Table 3 and the corresponding fibre distributions of the 20 % birch pulp – PLA composite in Table 4. From the results it can be seen that the fibre cutting has been more intensive with higher fibre content. Morphologies of the composites analysed with SEM imaging are seen in Figures 2 (40 wt% fibres) and 3 (20 wt% fibres), showing some gaps and disconnected fibres in addition to fibre breakage. The experimental stress-strain curves are shown in Figures 4 and 5 and the yield strength values presented in Table 7. Higher fibre content provides higher stress at break for the PLA matrix with lower elongation. The experimental tensile strength was 51.9 MPa with standard deviation 1.2 MPa for the 20% wt% fibres composite and 63.2 MPa with standard deviation 1.8 MPa for the 40% wt% fibres composite.

Calculations by the analytic methods for short fibres

The elastic values of the two composites calculated by Pan's approach are shown in Table 6.

Table 7 shows the stiffness and yield strength of the composites predicted by the short fibre theory compared to the experimental values. The failure mode in 20 % birch pulp fibre – PLA composite is assumed to be fibre breaking. The fibres are considered fully aligned. The strength of each fraction calculated by the short fibre theory is shown

14

in Table 8. The average strength obtained for the 20% birch pulp – PLA composite is thus $\sigma_c^* = 52.9$ MPa.

Calculations by the Finite Element Method

The stiffness of the 40 % birch pulp – PLA was calculated from the FE models and compared with the experimental value. Table 9 shows the stiffness of the composite calculated from different two phase FE models compared to the average value from the experiments. The E modulus of the fibres was varied between 30 and 42 GPa. The stress-strain state in 2D differs from that in 3D according to the plane stress or plane strain constitutive relations [31]. In order to quantify the effect of using 3D or 2D material input some of the plane strain models used the original 3D input moduli and Poisson's ratios of the fibres and matrix whereas the other plane strain models utilised input values transformed from 3D to 2D by equations 11 and 12 below [31]. The composite results of all plane strain models were transformed from 2D to 3D by using equations 11 and 12 backwards. In the plane stress models neither transformation is necessary. In the plane strain models with both transformations the error in stiffness was between 2 and 17% with E modulus 32 GPa giving errors between 2 and 8 %. In the plane strain models where the original 3D moduli and Poisson's ratio were used but the composite results were transformed from 2D to 3D the error was between 5 and 13 %. In the plane stress models the error was between 8 and 13 %. With fibre modulus 37 GPa the error in the plane stress model was 11 % and with fibre modulus 32 GPa 13 %.

$$E_{2D} = E_{3D}/(1 - v_{3D}^2) \tag{11}$$

$$v_{2D} = v_{3D}/(1 - v_{3D}) \tag{12}$$

The Poisson's ratios obtained from the FE models are also shown and compared to values obtained by the Rule-Of-Mixtures (ROM) in table 9.The difference to ROM is clear in models with high modulus of the fibres. This is partially because the fibres are not fully aligned in the loading direction and partially because they act both in series and in parallel with the matrix while the ROM assumes that the fibres and matrix act in parallel. Thus in soft matrix the stiff fibres move and orient in the loading direction and on the other hand the matrix elongates more than it could if the fibres were acting only parallel with the matrix.

Figure 8(a) shows as a contour plot the von Mises stress distribution in a small area of a two phase model and figure 8b the maximum principal strain distribution. Figure 10(a) shows a contour plot of the von Mises stress distribution in a small area of the best three phase model and figure 10(b) the material distribution in the area. The maximum von Mises stress in the three phase model is 1187 MPa while the overall stress of the composite is 80 MPa. This very high stress is limited to very small area. Stresses in the range of 300 - 400 MPa occur in a somewhat larger area at narrow ligaments of the fibres. When the overall strain of the composite is 1.5 % the maximum principal strain in the model is about 12.5 %, while strains in the range of 3.5 - 5 % occur in somewhat larger areas between fibres.

The stress-strain curve obtained from the three-phase plane strain model with the best parameter set (E fibre 30 GPa, E matrix 3771 MPa, E border 10 GPa, transformed to 2D i.e.in the model E fibre 31250 MPa, E matrix 4144 MPa, E border 10989 MPa, matrix and border modelled with plasticity) is compared to experimental stress-strain curves (in Figure 11). The elastic modulus prediction of this model was 8139 MPa

(about 2 % error). Figures 12(a-f) show the statistical von Mises stress, strain in the loading direction and equivalent plastic strain distributions and cumulative distributions from the best three phase model.

Discussion

Stiffness prediction

The stiffness calculated by Pan's method (Table 6) is very close to the experimental value for both fibre volume fractions (0.2 % and 4.9 % error). Also the FE models (Table 9) gave rather accurate stiffness predictions (2 – 17 % error in plane strain models with both transformations and 5 – 13 % error in plane stress models). As the elastic modulus of the fibres is not known very accurately, it had to be varied to see the effect on the composite modulus. The models are not very sensitive to the elastic modulus of the fibres, but they are rather sensitive to the elastic modulus of the matrix. This is natural as most of the deformation occurs in the soft matrix.

Stress-strain curves and strength prediction

It is clear from Tables 3 and 4 that only the longest fibre fractions can strengthen the composite. In both composites the more longitudinal fibres will tend to break and the more transverse fibres tend to fail at the interface. The SEM images show that some fibres did break and in some others the interface failed in shear (see figures 2a, 2b, 3a and 3b). This is because the fibre orientations and lengths vary greatly.

The yield strength for the 20 % birch pulp – PLA composite as estimated by the short fibre theory is very close to the experimental value (about 2 % error). In this composite there is not a clear yield stress though (see Figure 5), but gradual degradation of stiffness followed by rather abrupt plateau at the ultimate strength 62.7 MPa. The fact

that the ultimate strength is not larger than the yield strength could be explained partially by the small amount of fibres long enough to break and abrupt fracture of the aligned fibres and partially by the fact that a small fibre volume fraction does not cause much crack blunting and crack zigzagging.

The dominant failure mode of the 40 % birch pulp – PLA composite is assumed to be interface failure in transverse tension. Thus the strength cannot be calculated with the short fibre theory without a statistical distribution of fibre orientations and more information on bond strength. The statistical distribution of fibre orientations could be obtained from the 3D tomographic image, but in this small project there was no time for that. There is no clear yield stress in the 40 % birch pulp - PLA composite, but gradual degradation of stiffness, which is natural as the fibre angles are large and vary a lot. When the fibres break or de-bond one by one, the stiffness of the composite gradually degrades. The ultimate strength in this composite is 74.1 MPa, which is considerably larger than the yield stress. This could be partially explained by the larger amount of fibres compared to the 20% birch pulp - PLA composite, of which some are long enough to break even if not very well aligned, and partially by fracture mechanical effects like crack blunting caused by the fibres and large crack surface area caused by the crack zigzagging between the fibres. Also the strain at ultimate stress is in the same range in both composites (see Figures 2 and 3) and in a stiffer material with same strain the stress is naturally higher.

The three phase FE model

From the results of the two phase FE model (see Figures 8(a) and 8(b)) it can be seen that the highest stresses occur at the fibres and the largest strains in the matrix at narrow gaps between the fibres. A serious problem with these FE models is that in real life the

bond between the fibres and matrix is not perfect. In these composites without bond-enhancing agents the bond was rather poor. The two phase models did not take this into account. In later models a third material phase was created between the fibres and the matrix utilising modern image analysis tools (Figure 9). From Figures 10(a) and 10(b) one can see that the highest stresses occur in the narrow parts of the fibres and especially places where the fibres are attached to each other with only small ligaments. It is possible though that some of these are artefacts caused by the image analysis based 2D FE model generation. A 3D model would give more information on this. The local stresses and strains in the model are much larger than the overall stresses and strains of the composite, and above the strength of the fibres and the failure strain of the matrix respectively. This is caused by the facts that the fibres were modelled as elastic and isotropic, the matrix and interphase as elastic-plastic, details of the interphase (local initial debonds etc.) were not modelled, the composite and model were loaded to ultimate stress and damage and stress redistribution were not taken into account in the model. The maximum von Mises stress in the three phase model was over 1000 MPa when the overall stress of the composite was 80 MPa. This high stress was limited to very small area and is probably an artefact. Stresses in the range of 300-400 MPa occur in a larger area in some ligaments of the fibres. The stresses in the model should not be taken as real stresses in the microstructure but they can give insight on the key features of the microstructure and key phenomena of the failure. The real correlation between stresses and strains in the model and failure in the experiments should be studied using models with more detailed information on the bond between the fibres and anisotropic elasticity (or even anisotropic elasto-plasticity) for the fibres together with experimental

testing utilising optical methods to obtain local strain measurements during the test. Damage might also be taken into account in the models.

Still, the best three phase FE model was able to predict the stress-strain curve of the 40% birch pulp – PLA composite with good accuracy (Figure 10). Also the fitted value for the stiffness of the fibres in this model was in the range obtained in literature [25].

A remaining problem is that the current models employ isotropic material properties for the fibres. As the fibres carry load primarily in their longitudinal direction the elastic modulus and Poisson's ratio of the longitudinal direction were chosen. Adding anisotropy into the numerous and nearly arbitrarily shaped fibres is difficult and it was not included this project.

Statistical study of stresses and strains

In the statistical strain distribution of the three phase model (Figure 12(c)) there are three peaks corresponding to the three phases (fibres, border and matrix) but in the equivalent plastic strain distribution (Figure 12(e)) only two as the fibres were modelled as elastic. If we have two composites with similar materials but different microstructure or architecture (fibre lengths, widths, orientations, fibre integrity, bond strength, agglomerations, fibre-fibre interactions, possibly also extra strengthening elements like natural fibres in different orientations) these figures can be used for comparing the composites to each other and taking systematic steps towards tailoring the materials towards improved properties and application performance. The microstructure or architecture that gives smaller stress levels in the fibres and border and smaller strain levels in the matrix and border is preferable as it indicates higher strength. The maximum stresses should not be used in such a comparison as they usually occur at

very small area and may even be artefacts caused for example by badly shaped elements, and unless the material is very brittle such a small stress concentration does not cause breaking of the specimen when of smaller size scale than that of the critical failure mechanism. A suitable percentile of the distribution should be used instead. In unpublished commercial projects of the authors a level around 99 % has been found to be suitable for many materials, but for WPCs this is still somewhat unmapped territory. The suitable probability level means that the stress level is reached at a large enough area to cause breaking of the material. The same problem is in the strain calculations as well, because in some narrow gaps between fibres the strains may grow very high in a small area. This should be studied further by combined modelling and experiments and finally it will be possible to derive microstructural stress intensity factors and strain intensity factors for predicting strength of the material from the microstructural model.

Further work

A more rigorous analytical approach would include a statistical distribution for the fibre angles, use some mixed mode failure criterion for the interface, and integrate over the distributions to obtain the estimates. This would need an experimental value for the transverse tensile strength of the interface. The longitudinal tensile strength of the interface could be obtained from fibre pull-out tests and the shear stress could be calculated from Cox's theory. The tensile stresses could be taken as the applied strain transformed to the coordinate system along the fibre multiplied by matrix stiffness.

The FE approach used in this study is also very approximate. The real bond area and the Interfacial Shear Strength (ISS) between matrix and fibres are unknown and the anisotropy of the fibres is not included in the model. In further projects it is important to include more information of the fibre-matrix interface in the FE models. It is necessary

to study the bond areas between the fibres and the matrix more thoroughly. With fibre pull-out tests and optic or X-ray methods it is possible to find the properties of the border phase. Three-dimensional models based on micro tomographic images will give more information on the true stresses and strains in the composite. Additionally, the present models did not take viscoelasticity into account, which may have some effect on the stress-strain curves as the matrix material is highly viscoelastic. It is possible to add viscoelasticity in the models and compare to tensile tests at different loading rates. It would also be better to create the border phase so that it takes area from the matrix only and leaves the fibres intact. This would reduce the number of fitting parameters and enable more realistic treatment of the bond. In the long run it will be possible to tailor WPC composites and rank different WPC microstructures and architectures using micro tomography based FE models and statistical study of the stresses and strains.

The local stresses and strains and the strength indicative probability levels in stress and strain-distributions should be studied further by combined modelling and experiments. This would enable derivation of microstructural stress intensity factors for predicting strength from the microstructural models in all loading directions, and even under combined loadings from the microstructural models. Those microstructural stress/strain intensity factors would be perfect tools for engineers designing with WPCs and would thus promote sales of WPC materials. This kind of study would also enable optimization of microstructures of WPCs and hybrid WPCs that contain more phases, for example added natural fibres, and developing new high-strength materials with desired amount of ductility.

These composites as such are feasible only for limited applications. The fibres are too short and the Interfacial Shear Strength too small. Additionally, the fibres are not

well aligned. By using some coupling agent, for example MAPP (Maleic Anhydride grafted PolyPropylene) [32, 33] it is possible to increase the ISS. The cutting forces in mixing screw during compounding and injection moulding break the fibres too short. If the fibres could somehow be protected against this premature breaking during processing, or the compounding and injection moulding process stages could be improved to reduce fibre breakage, it would be possible to create stronger composites. As this is difficult, possibly the main asset in order to strengthen WPCs is related to interaction between matrix and fibres combined with proper distribution of the fibres. Malkapuram et al. [33] list several possible methods for modifying natural fibres to be used in polymer composites.

Summary

This work presents methodology of assessing stiffness and strength of Wood Plastic Composites with the theory of short fibre composites and with tomography based Finite Element modelling. The most critical further steps needed in order to fully assess the stress-strain behaviour, strength and stiffness of WPCs are discussed and a FEM assisted way of comparing WPC microstructures is presented. Accurate stiffness predictions were obtained: errors were in the range of 5 % with the short fibre theory and with the best FE models. Strength prediction was also very good with 2 % error in the case of reasonably well aligned fibres. With the FE method even the stress-strain curve of the composite was obtained with good accuracy. Still, this study contained some fitting due to insufficient data on the fibre-matrix interface. This information must be obtained experimentally to be able to give fully reliable strength and stress-strain curve predictions. Presenting modelled stresses and strains as statistical distributions enables comparison of different microstructures and architectures. In the future it will

be possible to optimise composites and predict strength of WPCs using microstructural stress/strain intensity factors derived from tomography based FE models.

The applied material systems were simplified for the case study. They are feasible as such only for limited applications. The fibres are too short and the ISS too small. By using coupling agents it is possible to increase ISS. Different wood species and processing systems would give different fibre length and width distributions. Architectures with added natural or synthetic fibres are also possible. There is still much room for research and development in structure and processing of WPCs, especially in improving strength and dimensional stability. The modelling methods presented here are good tools to be utilized as a part of this development.

Funding

Acknowledgements

Conflict of interest

None declared

References

1. Madsen B, Gamstedt K, Wood versus Plant Fibres: Similarities and Differences in Composite Applications, Advances in Material Science and Engineering, Vol 2013, Article ID 554346, 14 pages.

2. Mohanty AK, Misra M and Drzal LT, Natural Fibres, Biopolymers, and Biocomposites, CPR Press, Boca Raton, Fla, USA, 2005.

3. Petinakis E, Yu L, Simon G, Dean K, Natural Fibre Bio-Composites Incorporating Poly(Lactic Acid), Materials Science » Composite Materials » "Fibre Reinforced Polymers - The Technology Applied for Concrete Repair", book edited by Martin Alberto Masuelli, ISBN 978-953-51-0938-9, Published: January 23, 2013 under CC BY 3.0 license. © The Author(s). http://www.intechopen.com/books/fibre-reinforced-polymers-the-technology-applied-for-concrete-repair/natural-fibre-bio-composites-incorporating-poly-lactic-acid-

4. Dittenber DB, Ganga Rao HVS, Critical Review of Recent Publications on Use of Natural Composites in Infrastructure, Composites: Part A (2011), doi: 10.1016/j.compositesa.2011.11.019

5. Almgren KM, Wood-fibre composites: Stress transfer and hygroexpansion, Doctoral Thesis (2010), KTH Fibre and Polymer Technology, School of Chemical Sciences and Engineering, Royal Institute of Technology, Stockholm, Sweden

6. Peltola H, Pääkkönen E, Jetsu P, Heinemann S, Wood based PLA and PP composites: Effect of fibre type and matrix polymer on fibre morphology, dispersion and composite properties, Composites: Part A 61 (2014) 13-22

7. Chinga-Carrasco G, Miettinen A, Luengo Hendriks CL, Gamstedt, EK, Kataja M, (2011). Structural Characterisation of Kraft Pulp Fibres and Their Nanofibrillated

Materials for Biodegradable Composite Applications, Nanocomposites and Polymers with Analytical Methods, Dr. John Cuppoletti (Ed.), ISBN: 978-953-307-352-1, InTech, Available from: http://www.intechopen.com/books/nanocomposites-andpolymers-with-analytical-methods/structural-characterisation-of-kraft-pulp-fibres-and-their-nanofibrillatedmaterials-for-biodegradab

8. Joffre T, Structure and Mechanical Behaviour of Wood-Fibre Composites, Dissertation, Uppsala University, 2014, ISSN 1651-6214

9. Schwarzkopf M, Muszynski L, Nairn JA, Micromechanics of the Internal Bond in Wood Plastic Composites: Integrating Measurement and Modelling, 11th world Congress on Computational Mechanics, WCCM XI, July 20-25th, 2014, Barcelona, Spain

10. Schwarzkopf MJ, Characterization of Load Transfer in Wood-Based Composites, Dissertation (submitted), Oregon State University 2014

11. Madsen B, Joffe R, Peltola H, Nättinen K, Short cellulosic fibre/starch acetate composites - micromechanical modelling of Young's modulus, Journal of Composite Materials. Vol. 45 (2011) No: 20, 2119-2131

12. Eitzenberger J, Mechanics of microdamage development and stiffness degradation in fibre composites, Luleå University of Technology, Dept of Applied Physics and Mechanical Engineering, Division of Polymer Engineering, Licenthiate Thesis, (2007) 2007:69.

13. Lu Y, Mechanical properties of random discontinuous fibre composites manufactured from wetlay process, Virginia, Polytechnic Institute and State University, Engineering Mechanics, Master of Science Thesis, August 6, (2002).

14. Cox HL, The elasticity and strength of paper and other fibrous materials, *Br. J. Appl. Phys.*, No. 3, (1952), pp.72-79.

15. Nielson LE, *Mechanical properties of polymer and composites*, Vol. 2, Marcel Dekker, New York (1974).

16. Loewenstein KL, *Composite Materials*, Holliday and Elsevier, New York (1966).

17. Blumentritt BF, Vu BT and Cooper SL, Mechanical properties of Discontinuous Fibre Reinforced Thermoplastics. II. Random-in-Plane Fibre Orientation, *Polym. Eng. Sci.*, **15**(6) (1975), pp.428-436.

18. Christensen RM and Waals FM, Effective Stiffness of Randomly Oriented Fibre Composites, *J. Compos. Mater.*, **6**, (1972), pp. 518-532.

19. Manera M, Elastic properties of randomly oriented short fibre-glass composites, *J. Compos. Mater.*, **11**, (1977), pp. 235-247.

20. Pan N, The elastic constants of randomly oriented fibre composite: A new approach to prediction, *Sci. Eng. Compos. Mater.*, **5**(2) (1996), pp.63-72.

21. Curtis PT, Bader MG and Bailey JE, The stiffness and strength of a polyamide thermoplastic reinforced with glass and carbon fibres, *J. Mater. Sci.*, **13**, (1978), pp.377-390.

22. Chen PE, Strength Properties of Discontinuous Fibre Composites, *Polym. Eng. Sci.*, **11**(1) (1971), pp.51-56

23. Kelly A, and Tyson WR, *J. Mech. Phys. Solids*, **13**, (1965), pp.329-336.

24. Fu S-Y, and Lauke B, Effects of fibre length and fibre orientation distributions on the tensile strength of short-fibre-reinforced polymers, Compos. Sci. Technol., 56, (1996), pp. 1179-1190.

25. Neagu, http://www.forestprod.org/woodfibre05neagu.pdf, 15.12.2009. Not found on internet any more. See also Neagu R.C., Gamstedt E.K., Berthold F.: Stiffness Contribution of Various Wood Fibers to Composite Materials, *Journal of Composite Materials*, **40**, 8, (2006), pp. 663-699

26. Zhang P, Rogers J and Simonsen J, The relationship of interfacial shear strength to composite properties, 8th International Conference on Woodfibre-Plastic Composites (and other natural fibres).

27. Roberts RJ, Rowe RC and York P, The Poisson ratio of microcrystalline cellulose. *Int. J. Pharm.*, **105**, (1994), pp. 177-180.

28. Holmberg K, Laukkanen A, Ghabchi A, Rombouts M, Turunen E, Waudby R, Suhonen T, Valtonen K and Sarlin E, Computational modeling based wear resistance analysis of thick composite coatings, Tribology International, 72, (2014), pp. 13-30.

29. Holmberg K, Laukkanen A, Turunen E and Laitinen T, Wear resistance optimization of composite coatings by computational microstructural modeling, Surface and Coatings Technology, 247, (2014), pp. 1-13.

30. http://www.ctcms.nist.gov/oof/oof2/

31. Meille S, Garboczi EJ, Linear elastic properties of 2D and 3D models of porous materials made from elongated objects, Modelling Simul. Mater. Sci. Eng., Vol 9, 2001, pp. 371-390

32. Beg MDH and Pickering KL, Mechanical performance of Kraft fibre reinforced polypropylene composites: Influence of fibre length, fibre beating and hygrothermal ageing, *Composites Part A*, **39**, (2008), pp. 1748-1755.

33. Malkapuram R, Kumar V and Negi YS, Recent development in natural fibre reinforced polypropylene composites, *J. Reinf. Plas. Compos.*, Online First, November 20, (2008).

Tables

Table 1. Material parameters of the 40 % birch pulp – PLA composite

Fibre stiffness, E_f (MPa)	37000
Matrix stiffness, E_m (MPa)	3771
Poisson's ratio of the fibre, v_f	0.2
Poisson's ration of the matrix, v_m	0.3
Shear modulus of the matrix, G_m (MPa)	1450
Shear stress constant, τ_c (MPa)	4
Fibre length, l (mm)	0.025…0.06
Fibre radius, r (mm)	0.006…0.015
Axial failure stress of the fibre, σ_f^*	100
Stress in the matrix in fibre break, σ_m^*	63.9
Fibre volume fraction, V_f	0.4
Matrix volume fraction, V_m	0.6
Critical fibre length, l_c (mm)	0.14…0.36
Average fibre angle, θ_{avg} (deg)	46

Table 2. Material parameters of the 20 % birch pulp – PLA composite

Fibre stiffness, E_f (MPa)	37000
Matrix stiffness, E_m (MPa)	3771
Poisson's ratio of the fibre, v_f	0.2
Poisson's ration of the matrix, v_m	0.3
Shear modulus of the matrix, G_m (MPa)	1450
Shear stress constant, τ_c (MPa)	4
Fibre length, l (mm)	0.025…0.06
Fibre radius, r (mm)	0.006…0.015
Axial failure stress of the fibre, σ_f^*	100
Stress in the matrix in fibre break, σ_m^*	63.9
Fibre volume fraction, V_f	0.2
Matrix volume fraction, V_m	0.8
Critical fibre length, l_c (mm)	0.14…0.36
Average fibre angle, θ_{avg} (deg)	30

Table 3. Length, radius and critical length distributions (lrc) of 40% birch pulp – PLA composite

Length (mm)	Proportion (%)	Radius (mm)	lcr (mm)
< 0.05	2.16	0.006	0.143
0.05 - 0.1	27.28	0.006	0.143
0.1 - 0.15	33.77	0.009	0.214
0.15 - 0.2	16.98	0.009	0.214
0.2 - 0.5	18.06	0.0125	0.298
> 0.5	1.82	0.015	0.357

Table 4. Length, radius and critical length distributions (lcr) of 20% birch pulp – PLA composite

Length (mm)	Proportion (%)	Radius (mm)	lcr (mm)
< 0.05	0.95	0.006	0.143
0.05 – 0.1	17.94	0.006	0.143
0.1 - 0.15	24.89	0.009	0.214
0.15 – 0.2	28.37	0.009	0.214
0.2 – 0.5	24.51	0.0125	0.298
> 0.5	3.38	0.015	0.357

Table 5. The plastic model of the PLA matrix

Stress (MPa)	Plastic strain (%)
16.5	0
23	5.30E-04
30	9.09E-04
37	1.29E-03
43	1.97E-03
52	4.24E-03
62	6.21E-03
63	7.91E-03
80	9.90E-01

Table 6. The elastic values of the birch pulp – PLA composites predicted by Pan's method

Fibre volume fraction (%)	$E_1=E_2$ (MPa)	G_{12} (MPa)	ν_{12}
40	8002	3108	0.287
20	5886	2275	0.294

Table 7. The measured and predicted stiffness and yield strength for the birch pulp – PLA composites

Fibre volume fraction (%)	Predicted stiffness (MPa)	Measured stiffness (MPa)	error (%)	Predicted strength (MPa)	Measured strength (MPa)	error (%)
40	8002	8018	0.2		63.2	
20	5886	5617	4.9	52.9	51.9	1.9

Table 8. Strengths of the composite fractions corresponding to the fibre length fractions in 20% birch pulp – PLA composite (failure mode fibre breaking)

Fibre length l (mm)	Fibre radius r	Yield strength (MPa)	Fraction (%)
0.025 (<0.05)	0.006	41.7	2.2
0.075 (0.05-0.1)	0.006	48.3	27.3
0.125 (0.1-0.15)	0.009	49.5	33.8
0.175 (0.15-0.2)	0.009	53.9	17.0
0.35 (0.2-0.5)	0.0125	44.8	18.1
0.6 (>0.5)	0.015	50.1	1.8

Table 9. Stiffness calculated from 2D FE models compared to the experimental value

model	assumption	Ef, Em type	Efiber	Ematrix	v2D	v3D	E2D	E3D	vROM	v diff (%)	E error (%)
midq1	plane stress	original 3D	32000	3771	0.2806	0.2806	6933	6933	0.2873	-2	-13
midq2	plane stress	original 3D	37000	3771	0.2812	0.2812	7157	7157	0.2873	-2	-11
midq3	plane stress	original 3D	42000	3771	0.2816	0.2816	7346	7344	0.2873	-2	-8
midq4	plane strain	original 3D	32000	3771	0.3744	0.2724	7558	6997	0.2873	-5	-13
midq5	plane strain	original 3D	42000	3771	0.2573	0.2046	7895	7565	0.2873	-29	-5
topq1	plane strain	original 3D	37000	3771	0.3508	0.2597	7869	7338	0.2873	-10	-8
topq2	plane strain	original 3D	42000	3771	0.3483	0.2583	8069	7531	0.2873	-10	-6
topq3	plane strain	original 3D	32000	3771	0.3535	0.2612	7636	7115	0.2873	-9	-11
topq1b	plane strain	2D	38542	4144	0.6148	0.3807	10397	8890	0.4054	-6	11
topq2b	plane strain	2D	43750	4144	0.6108	0.3792	10745	9200	0.4054	-6	15
topq3b	plane strain	2D	33333	4144	0.619	0.3823	9996	8535	0.4054	-6	7
botq1	plane strain	original 3D	37000	3771	0.3484	0.2584	7939	7409	0.2873	-10	-7
botq2	plane strain	original 3D	42000	3771	0.3457	0.2569	8146	7608	0.2873	-11	-5
botq3	plane strain	original 3D	32000	3771	0.3513	0.26	7694	7174	0.2873	-10	-10
botq4	plane strain	original 3D	30000	3771	0.3525	0.2606	7585	7070	0.2873	-9	-12
botq1b	plane strain	2D	38542	4144	0.6113	0.3795	10518	9005	0.4054	-6	13
botq2b	plane strain	2D	43750	4144	0.6069	0.3777	10885	9333	0.4054	-7	17
botq3b	plane strain	2D	33333	4144	0.6158	0.3811	10099	8632	0.4054	-6	8
botq4b	plane strain	2D	31250	4144	0.6177	0.3818	9913	8467	0.4054	-6	6

Figures

Figure 1. Tensile test specimens of birch pulp – PLA composites
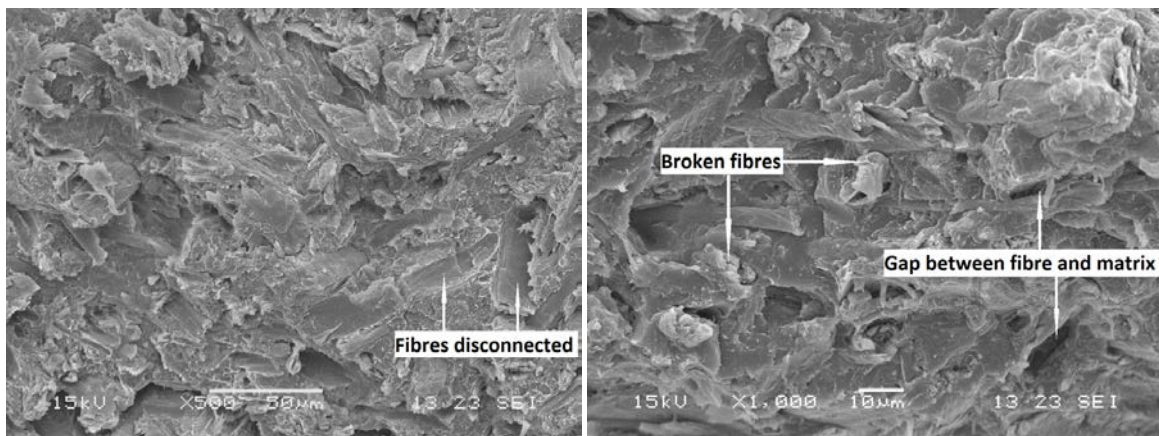
Figure 2. The 40 % birch pulp – PLA composite. a) 500 x, flat side of the specimen (process flow direction), b) 1000 x, cross-sectional surface in the middle of the sample
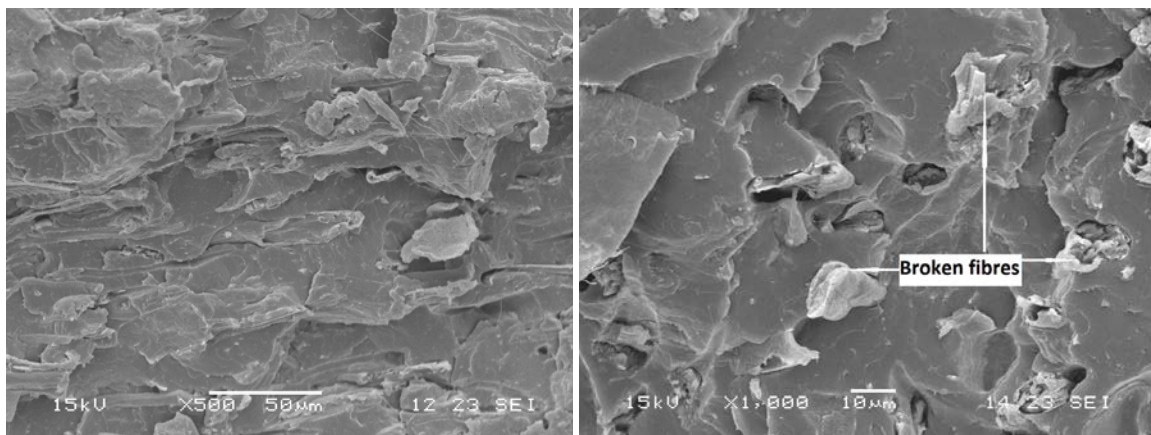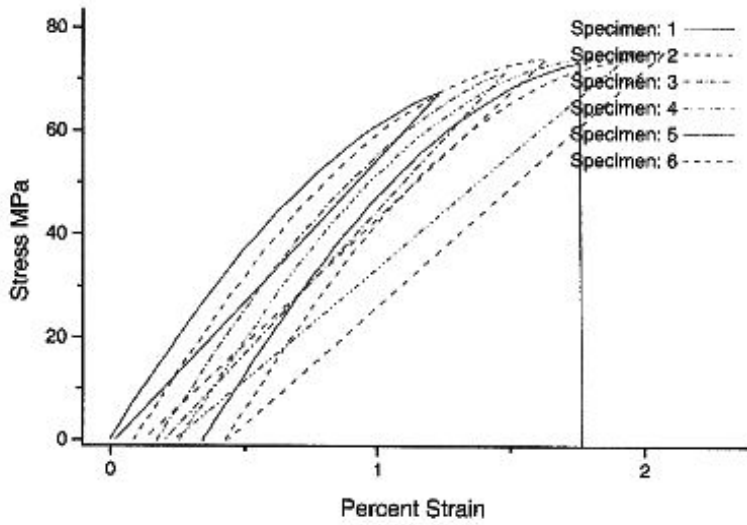

Figure 3. The 20 % birch pulp – PLA composite. a) 500 x, flat side of the specimen (process flow direction), b) 1000 x, cross-sectional surface in the middle of the sample

Figure 4. Experimental stress-strain curves of 40 % birch pulp – PLA composite
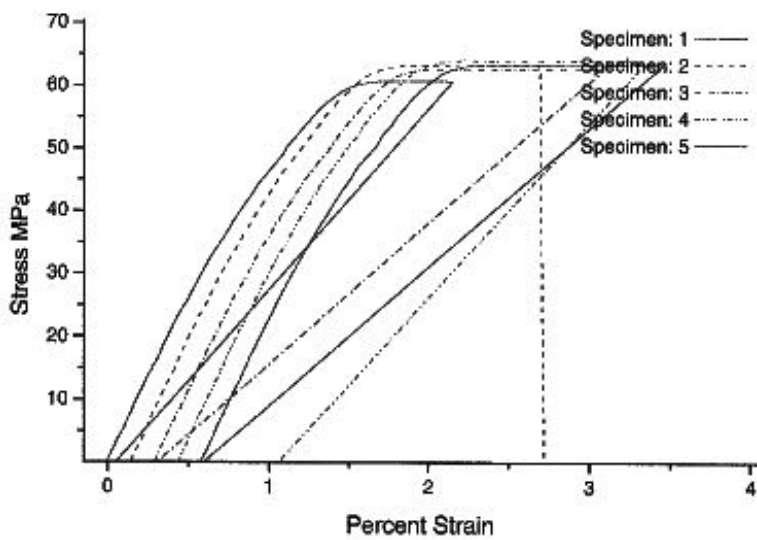
Figure 5. Experimental stress-strain curves of 20 % birch pulp – PLA composite

Figure 6. A part of a 2D image obtained by micro tomography
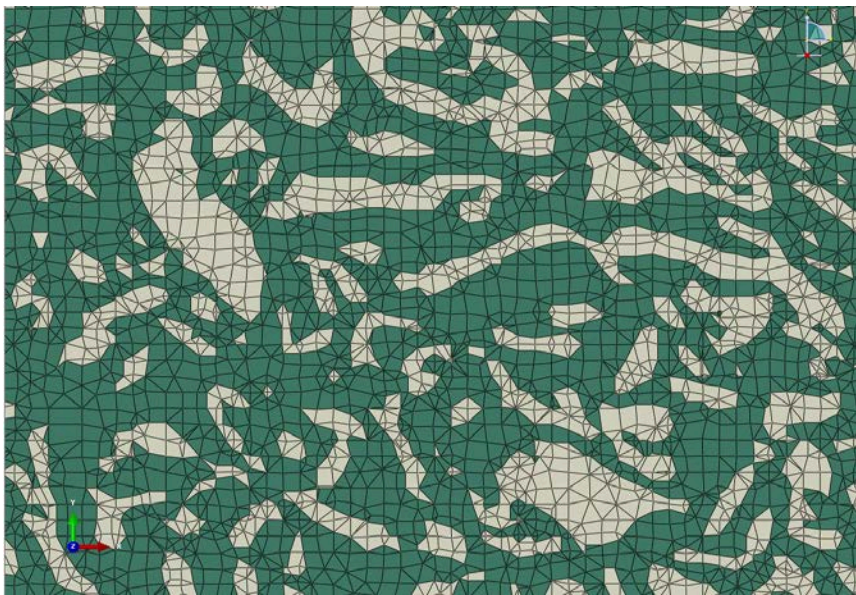
Figure 7. A part of a 2D mesh created from the micro tomography image (fig 6)
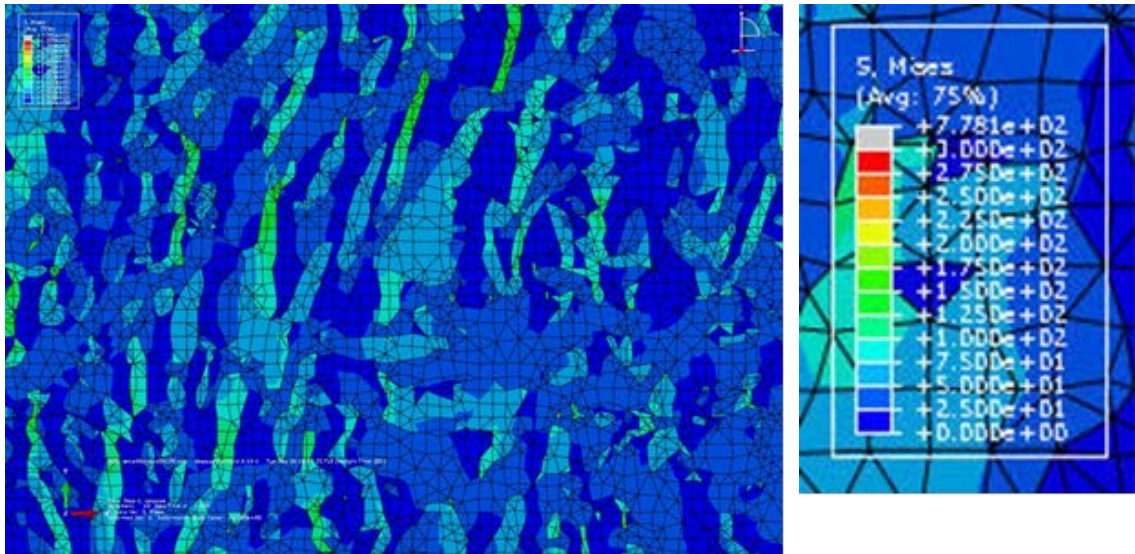
Figure 8(a). Von Mises stress distribution in a small area of a two phase model.
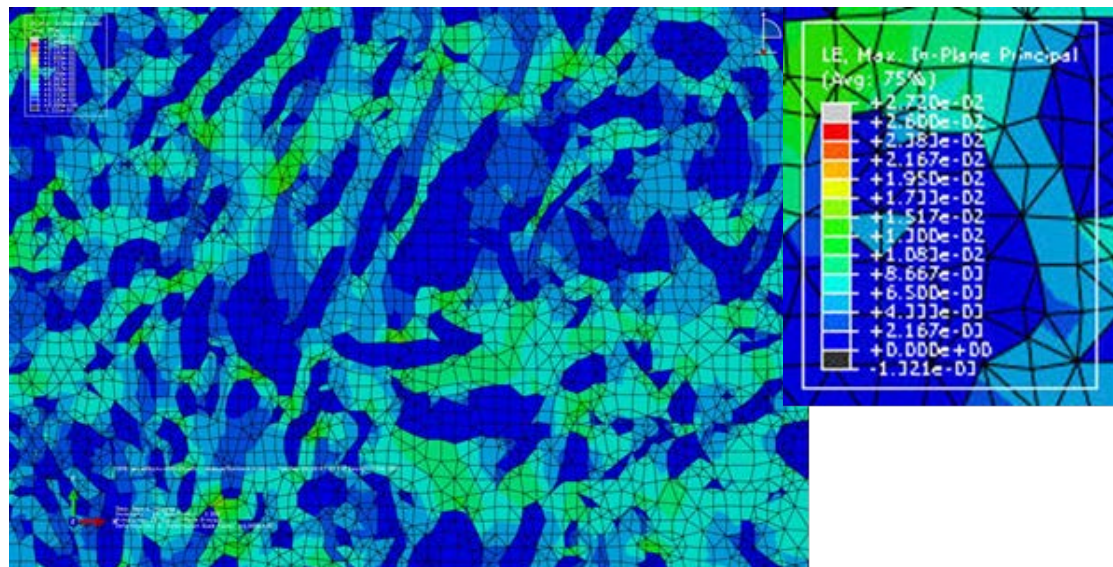
Figure 8(b). Maximum principal strain in the area of Figure 8(a).
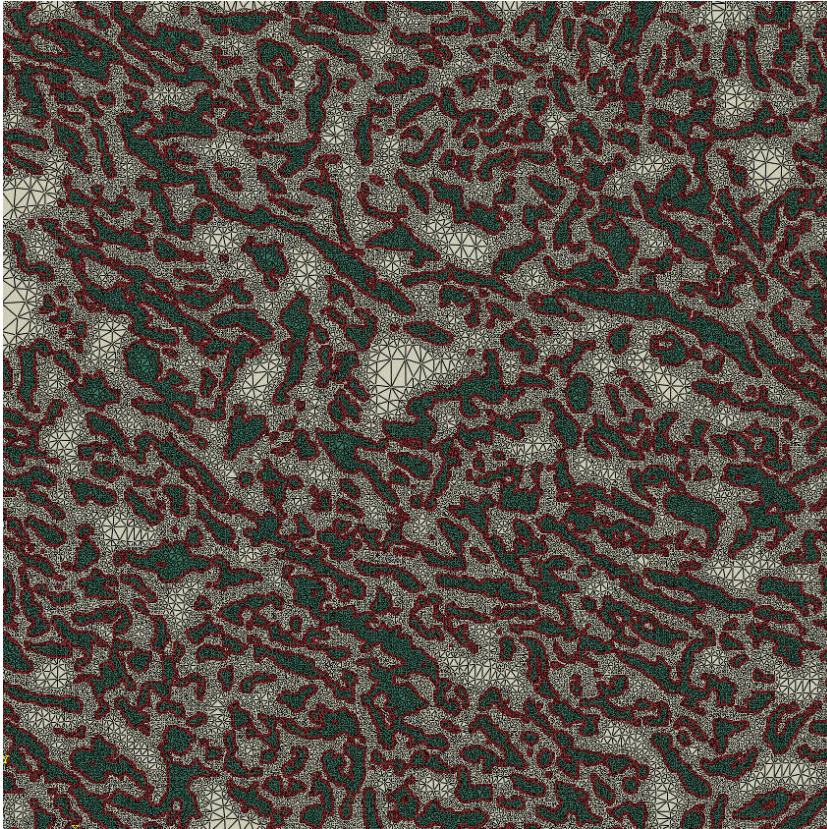
Figure 9. A model with three phases.
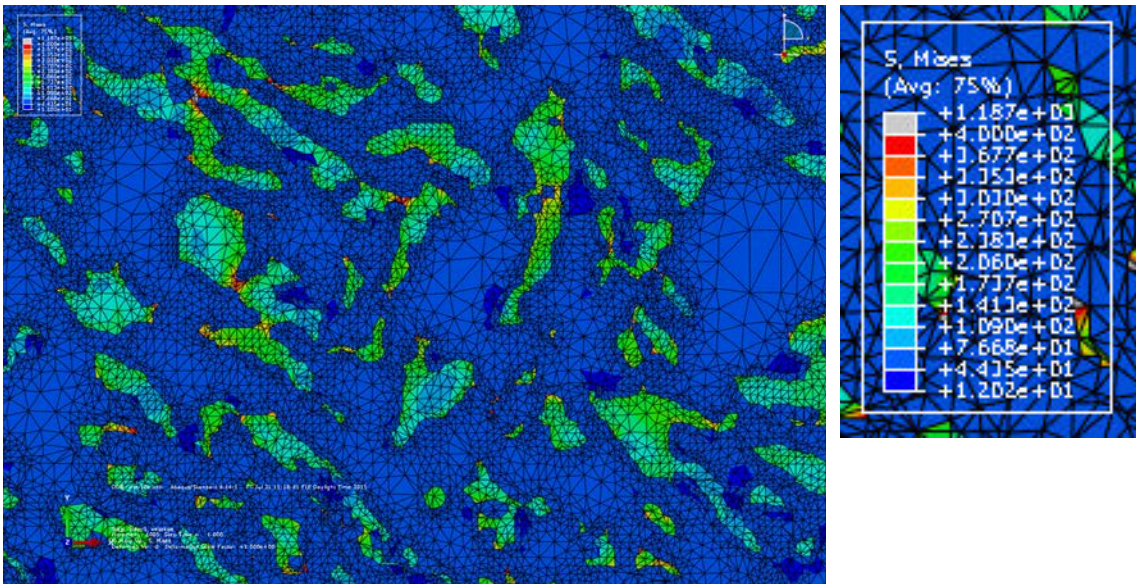
Figure 10(a). Von Mises stress distribution in a small area of the best three phase model
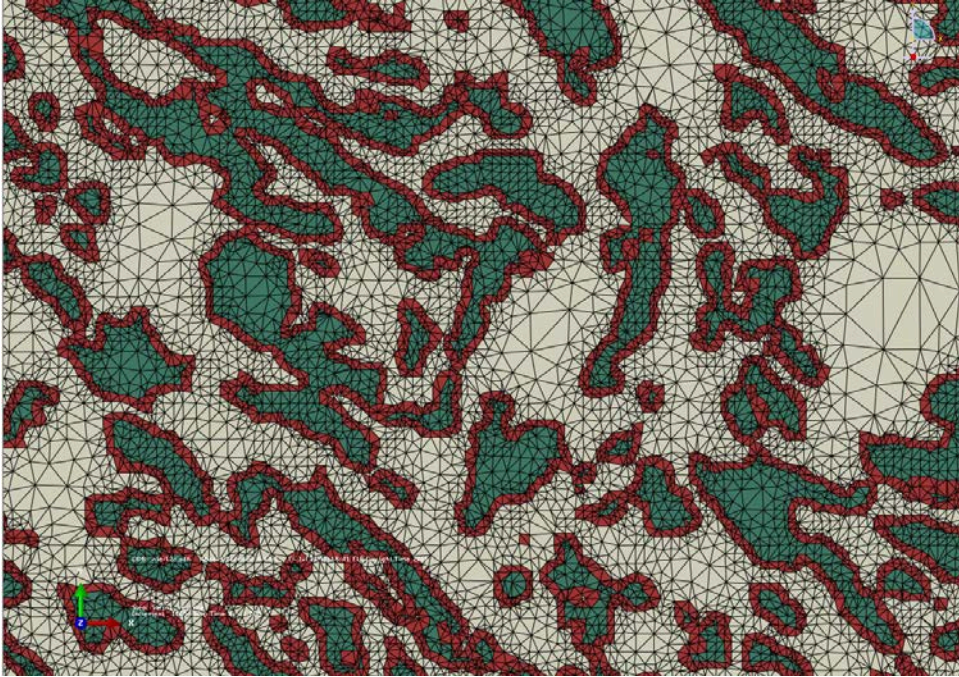
Figure 10(b). The material distribution in the area of Figure 10(a).
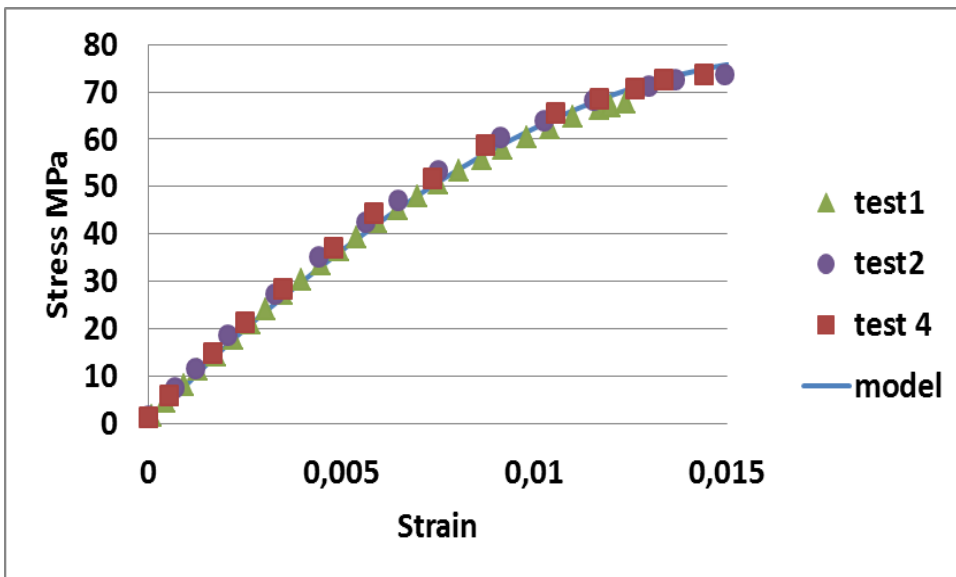
Figure 11. Stress-strain curve of the best three phase model compared to experiments.
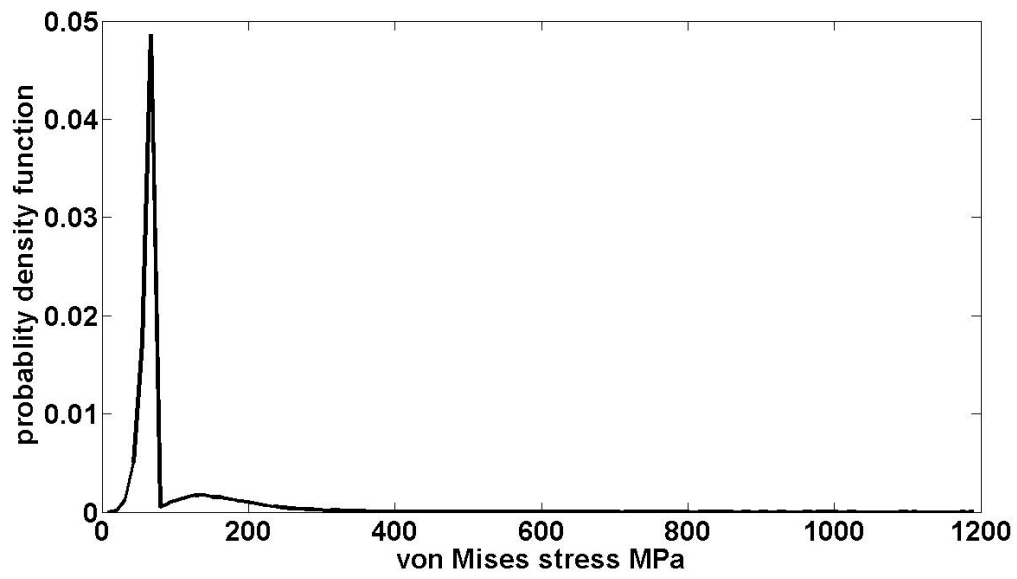
Figure 12(a). Von Mises stress distribution in the best three phase model.
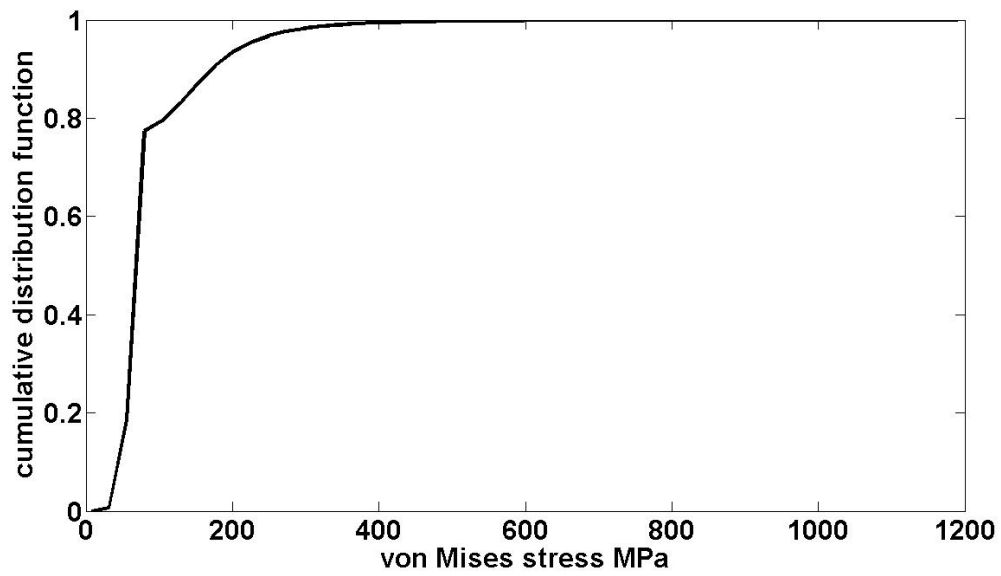
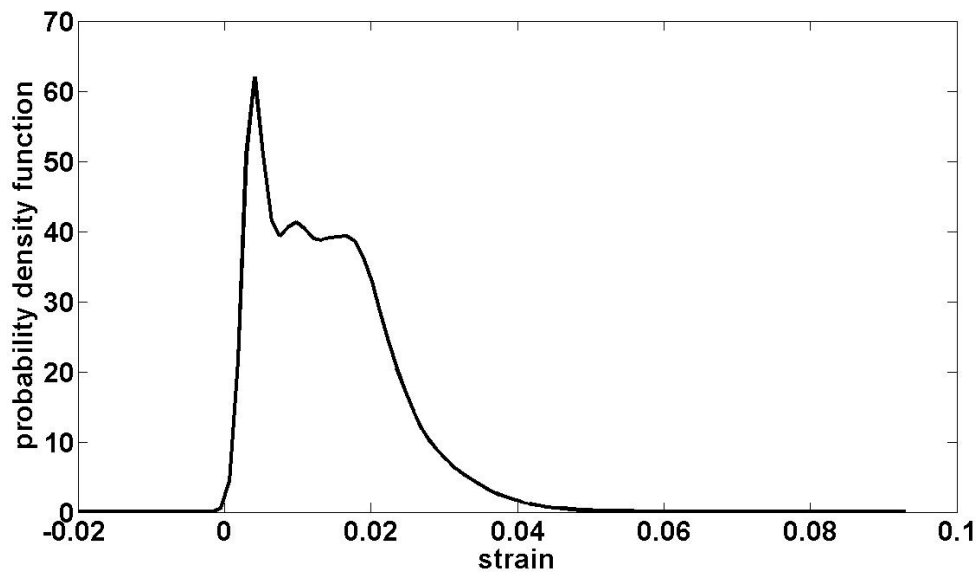**Figure 12 (b).** Von Mises stress distribution in the best three phase model (cumulative).

Figure 12(c). Strain in the loading direction distribution in the best three phase model.
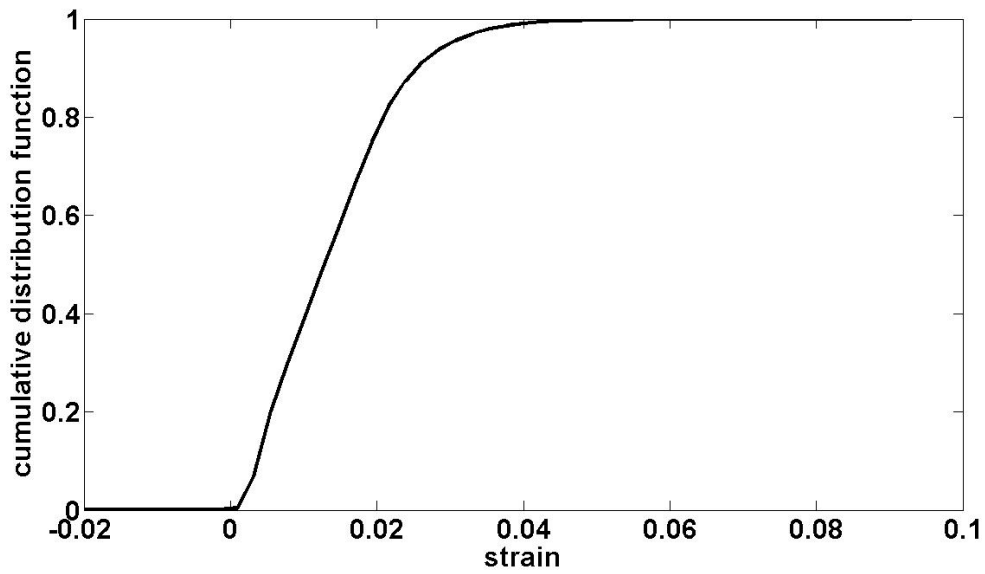

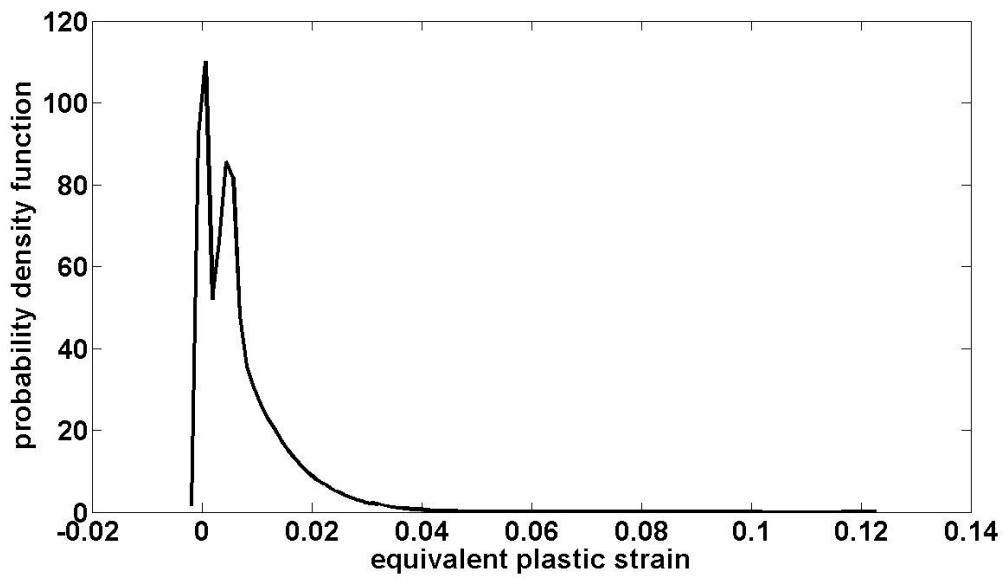**Figure 12(d).** Strain in the loading direction distribution in the best three phase model (cumulative).

Figure 12(e). Equivalent plastic strain distribution in the best three phase model.
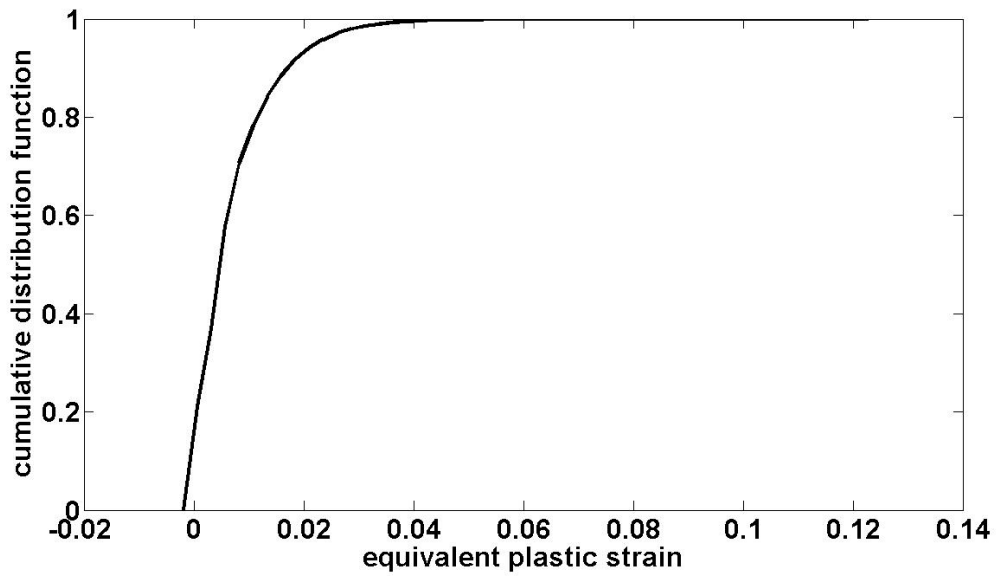

Figure 12(f). Equivalent plastic strain distribution in the best three phase model (cumulative).